
The Promises and Pitfalls of Deep Kernel Learning

Sebastian W. Ober¹

Carl E. Rasmussen^{1,2}

Mark van der Wilk³

¹Department of Engineering, University of Cambridge, Cambridge, United Kingdom

²Secondmind.ai, Cambridge, United Kingdom

³Department of Computing, Imperial College London, London, United Kingdom

Abstract

Deep kernel learning and related techniques promise to combine the representational power of neural networks with the reliable uncertainty estimates of Gaussian processes. One crucial aspect of these models is an expectation that, because they are treated as Gaussian process models optimized using the marginal likelihood, they are protected from overfitting. However, we identify pathological behavior, including overfitting, on a simple toy example. We explore this pathology, explaining its origins and considering how it applies to real datasets. Through careful experimentation on UCI datasets, CIFAR-10, and the UTKFace dataset, we find that the overfitting from overparameterized deep kernel learning, in which the model is “somewhat Bayesian”, can in certain scenarios be worse than that from not being Bayesian at all. However, we find that a fully Bayesian treatment of deep kernel learning can rectify this overfitting and obtain the desired performance improvements over standard neural networks and Gaussian processes.

1 INTRODUCTION

Gaussian process (GP) models [Rasmussen and Williams, 2006] are popular choices for Bayesian modeling due to their interpretable nature and reliable uncertainty estimates. These models typically involve only a handful of kernel hyperparameters, which are optimized with respect to the marginal likelihood in an empirical Bayes, or type-II maximum likelihood, approach. However, for most popular choices the kernel itself is fixed, meaning that GP models are unable to learn representations from the data that might aid predictions, and instead act mostly as smoothing devices. This greatly limits the applicability of GPs to high-dimensional and highly structured data, such as images.

Deep neural networks [LeCun et al., 2015], on the other hand, are known to learn powerful representations which are then used to make predictions on unseen test inputs. While deterministic neural networks have achieved state-of-the-art performance throughout supervised learning and beyond, they suffer from overconfident predictions [Guo et al., 2017], and do not provide reliable uncertainty estimates. The Bayesian treatment of neural networks attempts to address these issues; however, despite recent advances in variational inference (e.g. Ober and Aitchison [2020], Dusenberry et al. [2020]) and sampling methods (e.g. Heek and Kalchbrenner [2019], Zhang et al. [2019]) for Bayesian neural networks (BNNs), inference in BNNs remains difficult due to complex underlying posteriors and the large number of parameters in modern BNNs. Moreover, BNNs generally require multiple forward passes to obtain multiple samples of the predictive posterior to average over.

It is natural, therefore, to try to combine the uncertainty-representation advantages of Gaussian processes with the representation-learning advantages of neural networks, and thus obtain the “best of both worlds.” Indeed, many works have attempted to achieve this. In this paper, we focus on a line of work that we refer to broadly as *deep kernel learning* (DKL) [Calandra et al., 2016, Wilson et al., 2016b,a]. These works use a neural network to map inputs to points in an intermediate feature space, which is then used as the input space for a Gaussian process. The network parameters can be treated as hyperparameters of the kernel, and thus are optimized with respect to the (log) marginal likelihood, as in standard GP inference. This leads to an end-to-end training scheme that results in a model that hopefully benefits from the representational power of neural networks while also enjoying the benefits of reliable uncertainty estimation from the GP. Moreover, as the feature extraction done by the neural network is deterministic, inference only requires one forward pass of the neural net, unlike fully Bayesian BNNs.

In this work, we investigate to what extent DKL is actually able to achieve flexibility and good uncertainty. In particular, it is often claimed that optimizing the marginal likelihood

will automatically calibrate the complexity of the model, preventing overfitting (see e.g. Wilson et al. [2016b]). This claim is based on the common decomposition of the log marginal likelihood into “data fit” and “complexity penalty” terms [Rasmussen and Williams, 2006], which leads to the belief that a better marginal likelihood will result in better test performance. Here, we challenge this interpretation of the marginal likelihood for Gaussian processes with many hyperparameters, such as DKL, by showing that, in some cases, the overfitting from DKL models can be worse than that from a standard, deterministic neural network. This is because the marginal likelihood tries to correlate *all* the datapoints, rather than just those for which correlations will be important, and the neural network gives the model the flexibility to do so. As such, our work has implications for all GP methods which use highly parameterized kernels, as well as methods that optimize more than a handful of model parameters according to the marginal likelihood or ELBO.

2 RELATED WORK

Salakhutdinov and Hinton [2007] used deep belief networks to pretrain a neural network feature extractor to transform the inputs to a GP, with subsequent fine-tuning using the marginal likelihood. Calandra et al. [2016] removed the deep belief network pretraining and only used the marginal likelihood to train the model, referring to this as the “manifold GP.” Wilson et al. [2016b] improved the scalability of this model by using KISS-GP [Wilson and Nickisch, 2015], coining the term “deep kernel learning.” This was further extended to non-regression likelihoods and multiple outputs in Wilson et al. [2016a] by using stochastic variational inference [Hensman et al., 2015a] and Kronecker and Toeplitz structure [Wilson et al., 2015], resulting in stochastic variational deep kernel learning (SVDKL). These and related approaches which use the marginal likelihood to optimize the neural network parameters have been shown to be advantageous in multiple situations, including transfer testing and adversarial robustness [Bradshaw et al., 2017]. On the other hand, Tran et al. [2019] investigated poor calibration in these models, and proposed using Monte Carlo dropout [Gal and Ghahramani, 2016] to perform approximate Bayesian inference over the neural network weights in the model. However, they did not explain the poor calibration, nor did they identify the possibility of overfitting in DKL models.

Due to the difficulty of performing full inference over all BNN parameters, there has been a recent increase in interest in using deterministic feature extractors for models that only incorporate uncertainty in an output layer (e.g. Liu et al. [2020], van Amersfoort et al. [2020]). One of the most popular models in recent years has been the “neural linear” model [Riquelme et al., 2018, Ober and Rasmussen, 2019], which can be viewed as DKL with a linear kernel, or equivalently, Bayesian inference over the last layer of a neural network.

In particular, Ober and Rasmussen [2019] showed that it is difficult to get the neural linear model to perform well for regression without considerable hyperparameter tuning, and that fully Bayesian approaches for BNNs often require much less tuning to obtain comparable results.

3 BACKGROUND

3.1 GAUSSIAN PROCESSES

A Gaussian process is a collection of random variables such that every finite collection of these random variables is distributed according to a multivariate normal distribution. In the regression setting, where we have a dataset consisting of inputs $X = (x_1, \dots, x_N)^T$, $x_n \in \mathbb{R}^D$, and outputs $\mathbf{y} = (y_1, \dots, y_N)^T$, $y_n \in \mathbb{R}$, we assume that each datapoint is generated according to

$$y_n = f(x_n) + \varepsilon_n, \quad \varepsilon_n \sim \mathcal{N}(0, \sigma_n^2), \quad (1)$$

where f is drawn from a Gaussian process prior, $f \sim \mathcal{GP}(m, k)$. Here, $m : \mathbb{R}^D \rightarrow \mathbb{R}$ is the mean function, and $k : \mathbb{R}^D \times \mathbb{R}^D \rightarrow \mathbb{R}$ is a symmetric, positive semi-definite covariance (kernel) function. Together, these uniquely define the Gaussian process prior: for instance, the marginal distribution indexed by X is distributed according to $\mathcal{N}(\mathbf{m}(X), K)$, where $\mathbf{m}(X) = (m(x_1), \dots, m(x_N))^T$ and we define the kernel matrix $K := K(X, X)$, so that $K_{ij} = k(x_i, x_j)$. Predictions of the latent function for a collection of test points X_* can be computed in closed form:

$$\begin{aligned} \mathbf{f}_* | X, \mathbf{y}, X_* &\sim \mathcal{N}(\boldsymbol{\mu}_*, \boldsymbol{\Sigma}_*), \quad \text{where} & (2) \\ \boldsymbol{\mu}_* &= \mathbf{m}(X_*) + K(X_*, X)(K + \sigma_n^2 I_N)^{-1}(\mathbf{y} - \mathbf{m}(X)), \\ \boldsymbol{\Sigma}_* &= K(X_*, X_*) - K(X_*, X)(K + \sigma_n^2 I_N)^{-1}K(X, X_*). \end{aligned}$$

For the purposes of this work, we take the mean function to be zero.

Finally, it is typical for the kernel to have a number of hyperparameters which are learned along with the noise variance, σ_n^2 , by maximizing the (log) marginal likelihood (LML; also known as the model evidence), in an empirical Bayes, or type-II maximum likelihood approach:

$$\begin{aligned} \log p(\mathbf{y}) &= \log \mathcal{N}(\mathbf{y} | \mathbf{0}, K + \sigma_n^2 I_N) & (3) \\ &\stackrel{c}{=} \underbrace{-\frac{1}{2} \log |K + \sigma_n^2 I_N|}_{(a) \text{ complexity}} - \underbrace{\frac{1}{2} \mathbf{y}^T (K + \sigma_n^2 I_N)^{-1} \mathbf{y}}_{(b) \text{ data fit}}, \end{aligned}$$

where we note that (a) and (b) are often referred to as the “complexity penalty” and “data fit” terms, respectively. For the purposes of this work, we use the automatic relevance determination (ARD) squared-exponential (SE) kernel, $k(x, x') = \sigma_f^2 \exp(-\frac{1}{2} \sum_{d=1}^D (x_d - x'_d)^2 / l_d^2)$. Therefore, the hyperparameters to tune are the noise variance, σ_n^2 , signal variance, σ_f^2 , and lengthscales l_d^2 .

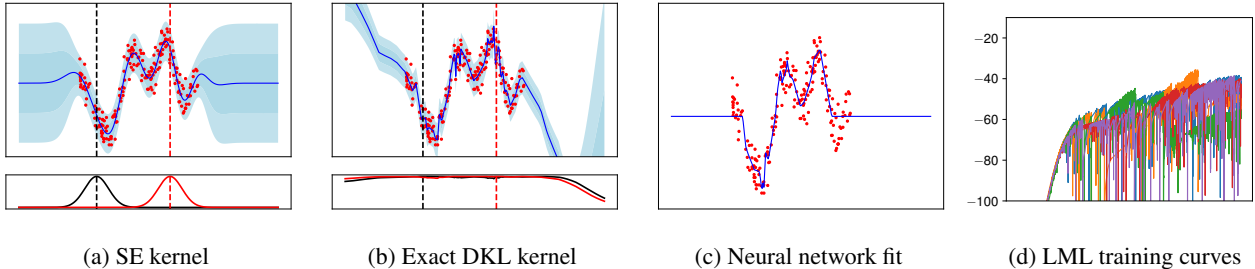


Figure 1: Results on the toy dataset from Snelson and Ghahramani [2006]. (a) and (b) show plots of the predictive posterior for squared exponential (SE) and deep kernel learning (DKL) kernels, respectively; below each plot we also plot correlation functions $\rho_{x'}(x) = k(x, x')/\sigma_f^2$ at two points x' given by the vertical dashed lines. (c) shows the fit given by the neural network analogous to the DKL model. Finally, (d) shows training curves of the log marginal likelihood (LML) for 5 different initializations of DKL.

3.2 DEEP KERNEL LEARNING

One of the central critiques of Gaussian process regression is that it does not actually learn representations of the data. In an attempt to address this, several works [Calandra et al., 2016, Wilson et al., 2016b,a, Bradshaw et al., 2017] have proposed variants of deep kernel learning (DKL), which maps the inputs x_n to intermediate values $v_n \in \mathbb{R}^Q$ through a neural network $g_\phi(\cdot)$ parameterized by weights and biases ϕ . These intermediate values are then used as inputs to the standard kernel resulting in the effective kernel $k_{DKL}(x, x') = k(g_\phi(x), g_\phi(x'))$. In order to learn the network weights and thereby learn representations of the data, it was proposed to maximize the marginal likelihood with respect to the weights ϕ along with the kernel hyperparameters. We denote all the hyperparameters by $\theta := \{\phi, \sigma_n, \sigma_f, \{l_q\}_{q=1}^Q\}$.

3.3 STOCHASTIC VARIATIONAL DEEP KERNEL LEARNING

The proposed deep kernel learning model suffers from two major drawbacks. First, due to the $\mathcal{O}(N^3)$ computational complexity of GPs, the standard DKL model suffers from poor scalability in the number of data.¹ Second, exact GP inference is only possible for Gaussian likelihoods, and therefore approximate techniques must be used for classification. To achieve both, we follow Bradshaw et al. [2017] in using stochastic variational inference (SVI) for GPs as introduced in Hensman et al. [2015a], to result in stochastic variational DKL (SVDKL).²

Considering the case of C multiple outputs, we first introduce M latent inducing variables $\mathbf{u}_c = (u_{c1}, \dots, u_{cM})^T$, in-

¹We note that Wilson et al. [2016b], which was the first paper to use the terminology “DKL”, attempted to address scalability using KISS-GP [Wilson and Nickisch, 2015]; however, we use “DKL” to refer to the model with exact GP inference.

²We note again that this is slightly different in exact implementation to the SVDKL model proposed in Wilson et al. [2016a].

dexed by M inducing inputs $z_m \in \mathbb{R}^Q$, which lie in the feature space at the output of the neural network. We assume the standard variational posterior over the inducing variables, $q(\mathbf{u}_c) = \mathcal{N}(\mathbf{m}_c, \mathbf{S}_c)$, leading to an approximate posterior $q(\mathbf{f}, \mathbf{u}) = p(\mathbf{f}|\mathbf{u})q(\mathbf{u})$. We optimize the variational parameters \mathbf{m}_c and \mathbf{S}_c , along with the model hyperparameters θ , jointly by maximizing the evidence lower bound (ELBO):

$$\mathcal{L} = \mathbb{E}_{q(\mathbf{u})p(\mathbf{f}|\mathbf{u})}[\log p(\mathbf{y}|\mathbf{f})] - D_{KL}(q(\mathbf{u})||p(\mathbf{u})). \quad (4)$$

Note that there are no restrictions on the likelihood $p(\mathbf{y}|\mathbf{f})$ as the first term can be estimated using Monte Carlo sampling with the reparameterization trick [Kingma and Welling, 2013, Rezende et al., 2014]. Finally, we note that given sufficient inducing points, the ELBO is “tight” enough in the sense that it can be used as a stand-in for the marginal likelihood for hyperparameter optimization [Burt et al., 2020].

4 PATHOLOGICAL BEHAVIOR IN A TOY PROBLEM

We first consider (exact) DKL on the toy problem from Snelson and Ghahramani [2006], a 1-dimensional regression problem consisting of 200 noisy input-output pairs generated from a GP with squared exponential kernel. We consider DKL using a two hidden-layer fully-connected ReLU network with layer widths [100, 50] as the feature extractor, letting $Q = 2$ with a squared exponential kernel for the GP.³ We describe the architecture and experimental details in more detail in Appendix B.

We plot the predictive posteriors of both a baseline GP with an SE kernel (corresponding to the ground truth), and DKL in Figures 1a and 1b, respectively. We additionally compare to the fit given by the deterministic neural network corresponding to using the same feature extractor as the DKL model, so that both models have the same depth. To ensure

³We note that this is a smaller feature extractor than that proposed for a dataset of this size in Wilson et al. [2016b].

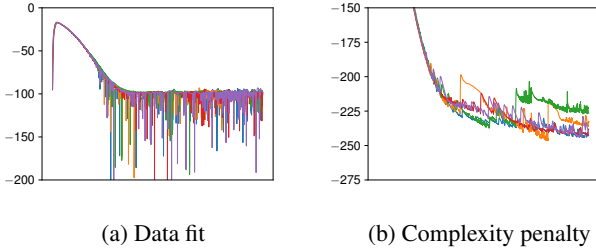


Figure 2: Training curves for the data fit and complexity penalties of the log marginal likelihood for the toy problem.

a fair comparison, we retain the same training procedure, using the same learning rates, full batch training, and number of optimization steps, so that we only change the model and training loss (from the LML to mean squared error). We observe that DKL suffers from pathological behavior: the fit is very jagged and extrapolates wildly outside the training data. Moreover, we show in App. C.1 that different initializations can give very different results, indicating that different local minima have very different generalization properties. On the other hand, the fit from the neural network, shown in Fig. 1c, does not show such extreme pathological behavior: while there is some evidence of overfitting, it is in general much less than that of DKL.

Finally, we plot training curves from five different runs of DKL in Fig. 1d. From these, we observe that training is very unstable, with many significant spikes in the marginal likelihood objective. We found that reducing the learning rate does improve stability, but only slightly (App. C.1). We also observe that each run often ends up settling in a different local minimum with very different final values of the log marginal likelihood.

In general, this behavior is very concerning: one would hope that adding a Bayesian layer to a deterministic network would improve performance, as introducing Bayesian principles is often touted as a method to reduce overfitting (e.g. Osawa et al. [2019]). However, based off this toy problem performance seems to worsen with the addition of a Bayesian layer at the output. As this finding is seemingly at conflict with most of the literature, which has found that DKL, or variations thereof, can be useful, we devote the rest of this work to understanding when and why this pathological behavior arises, including for real datasets.

5 UNDERSTANDING THE PATHOLOGY

To help understand the observed pathological behavior, we first look at the curves of the “data fit” and “complexity penalties” for five different initializations on the toy dataset. We present these curves in Fig. 2. We note that each of the data fit curves largely stabilize around -100 nats, so that the complexity terms seem to account for most of the difference

in the final marginal likelihood (Fig. 1d). This behavior is explained by the following proposition, which states that the data fit term becomes uninteresting for any GPs with learnable signal variance trained on the marginal likelihood.

Proposition 1. *Consider the Gaussian process regression model as described in Eq. 1. Then, for any valid kernel function that can be written in the form $k(x, x') = \sigma_f^2 \hat{k}(x, x')$, where σ_f^2 is a learnable hyperparameter along with learnable noise σ_n^2 (and any other kernel hyperparameters), we have that the “data fit” term will equal $-N/2$ at the optimum of the marginal likelihood.*

The proof (App. A) is achieved by simple differentiation with respect to σ_f . This result is far-reaching, applying to the vast majority of kernel choices that we are aware of. This proposition therefore implies that the division of the marginal likelihood into “data fit” and “complexity penalty” terms is in general unhelpful, as the data fit term becomes uninteresting after training and the complexity penalty is responsible for any difference in marginal likelihood for GPs with different kernels.

However, we can still consider what a lower complexity penalty means for the learned kernel. Recall that the complexity penalty is given by

$$\frac{1}{2} \log |K + \sigma_n^2 I_N| = \frac{N}{2} \log \sigma_f^2 + \frac{1}{2} \log |\hat{K} + \hat{\sigma}_n^2 I_N|. \quad (5)$$

Maximizing the marginal likelihood encourages this term to be minimized, which can be done in at least two ways: minimizing σ_f , or minimizing the $|\hat{K} + \hat{\sigma}_n^2 I_N|$. However, there is little freedom in minimizing σ_f , because that would compromise the data fit. Therefore, the main mechanism for minimizing the complexity penalty would be through minimizing the second term. One way of doing this is to correlate the input points as much as possible: if there are enough degrees of freedom in the kernel, it is possible to “hack” the Gram matrix so that it can do this while minimizing the impact on the data fit term. We see this by looking at the correlation plots for the SE and DKL fits in Fig. 1: below the plots of the predictive posteriors, we have plotted correlation functions $\rho_{x'}(x) = k(x, x')/\sigma_f^2$ at two points x' given by the vertical dashed lines. We see that, while Fig. 1a shows the expected Gaussian bump for the SE kernel, Fig. 1b shows near-unity correlation functions for all values. Furthermore, in Appendix C.1 we show empirically that for fits that do not show as much correlation, the final marginal likelihood is worse, suggesting that increasing the correlation is indeed the main mechanism by which the model increases its marginal likelihood.

These results suggest that adding flexibility to a GP can lead to pathological results, as the GP will use that flexibility to try to correlate *all* input points in the prior, not only the points where we would like correlations to appear. We now investigate how these observations relate to real, complex

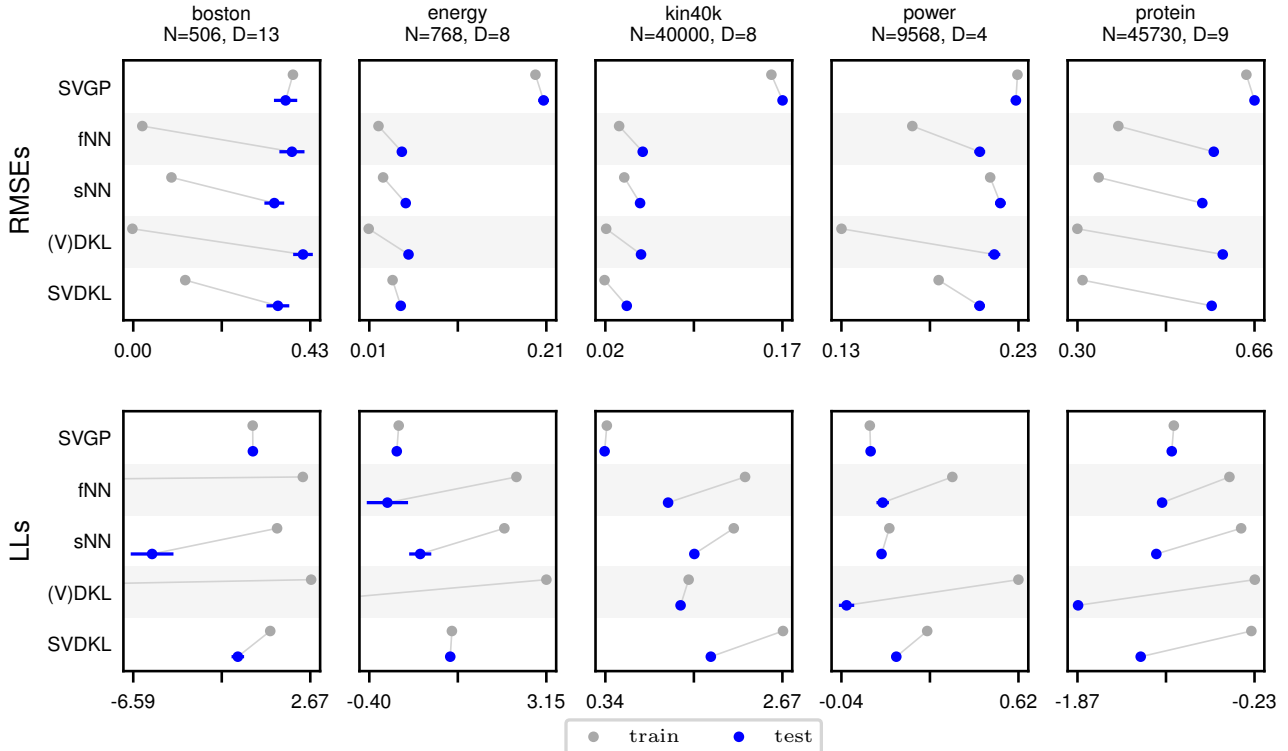


Figure 3: Results for the UCI datasets. We report train and test RMSEs and log likelihoods (LLs) for each method we consider, averaged over the 20 splits. Left is better for RMSEs; right is better for LLs. Error bars represent one standard error.

Table 1: LMLs/ELBOs per datapoint for UCI datasets.

	SVGP	(V)DKL	SVDKL
BOSTON	-1.66 ± 0.06	2.47 ± 0.00	0.47 ± 0.01
ENERGY	-0.07 ± 0.01	3.01 ± 0.02	1.21 ± 0.00
KIN40K	0.14 ± 0.00	1.41 ± 0.00	2.62 ± 0.00
POWER	0.01 ± 0.00	0.57 ± 0.00	0.25 ± 0.00
PROTEIN	-1.06 ± 0.00	-0.32 ± 0.01	-0.35 ± 0.00

datasets, as well as to the prior literature which has shown that DKL can obtain good results.

6 DKL FOR REAL DATASETS

We now consider experiments on various datasets and architectures to further investigate the observed pathological behavior. We provide full experimental details in Appendix B. In addition, we provide additional experimental results in Appendix C.

6.1 DKL FOR UCI REGRESSION

We first consider DKL applied to a selection of regression datasets from the UCI repository [Dua and Graff, 2017]:

BOSTON, ENERGY, KIN40K, POWER, PROTEIN. These represent a range of different sizes and dimensions: ENERGY, POWER, and PROTEIN were chosen specifically because we expect that they can benefit from the added depth to a GP [Salimbeni and Deisenroth, 2017].

We consider a range of different models. First, we consider a baseline stochastic variational GP (SVGP) model with an ARD SE kernel: we use 100 inducing points and a batch size of 32 for the small datasets (BOSTON, ENERGY) and 1000 inducing points and a batch size of 100 for the larger ones. We compare to a neural network trained with mean squared error loss and SVDKL using the same neural network architecture for feature extraction, as well as the same number of inducing points as for SVGP. We use an architecture of [50, 50] for the smaller datasets, and [1000, 500, 50] for the larger ones.⁴ For the neural networks, we train both with full batch training (full neural network; fNN) and minibatching with the same batch size as SVGP (stochastic neural network; sNN). Finally, for the smaller datasets, we compare to exact DKL, whereas for the larger ones we compare to full-batch SVDKL, which we term variational DKL (VDKL), as exact DKL is infeasible. For each deep method we also add the same small weight decay to help reduce overfitting,

⁴We note that these architectures are smaller than the ones proposed by Wilson et al. [2016b].

Table 2: Results for the image datasets, without data augmentation. We report means plus/minus one standard error.

	Batch size: 100					Batch size: 200/500		
	NN	SVDKL	pNN	fSVDKL	pSVDKL	pNN	fSVDKL	pSVDKL
UTKFace - ELBO	-	0.92 ± 0.01	-	1.05 ± 0.30	1.03 ± 0.10	-	0.75 ± 0.34	1.43 ± 0.04
Train RMSE	0.04 ± 0.00	0.04 ± 0.00	0.04 ± 0.00	0.08 ± 0.03	0.04 ± 0.00	0.04 ± 0.00	0.12 ± 0.03	0.04 ± 0.00
Test RMSE	0.40 ± 0.00	0.40 ± 0.01	0.41 ± 0.00	0.31 ± 0.07	0.38 ± 0.02	0.39 ± 0.01	0.23 ± 0.07	0.34 ± 0.02
Train LL	1.81 ± 0.01	1.30 ± 0.01	1.83 ± 0.01	1.16 ± 0.31	1.20 ± 0.08	1.83 ± 0.01	0.82 ± 0.34	1.60 ± 0.03
Test LL	-48.73 ± 1.64	-6.88 ± 0.38	-53.72 ± 1.71	-7.55 ± 3.42	-4.74 ± 1.35	-48.48 ± 2.07	-5.36 ± 4.78	-10.43 ± 2.94
CIFAR-10 - ELBO	-	-0.76 ± 0.28	-	-0.02 ± 0.00	-0.00 ± 0.00	-	-0.02 ± 0.00	-0.00 ± 0.00
Train Acc.	1.00 ± 0.00	0.76 ± 0.09	1.00 ± 0.00	1.00 ± 0.00	1.00 ± 0.00	1.00 ± 0.00	1.00 ± 0.00	1.00 ± 0.00
Test Acc.	0.79 ± 0.00	0.63 ± 0.03	0.79 ± 0.00	0.78 ± 0.00	0.79 ± 0.00	0.79 ± 0.00	0.79 ± 0.00	0.79 ± 0.00
Train LL	-0.00 ± 0.00	-0.71 ± 0.28	-0.00 ± 0.00	-0.01 ± 0.00	-0.00 ± 0.00	-0.00 ± 0.00	-0.00 ± 0.00	-0.00 ± 0.00
Test LL	-2.05 ± 0.03	-1.37 ± 0.10	-2.30 ± 0.11	-1.14 ± 0.00	-1.13 ± 0.01	-2.88 ± 0.04	-1.07 ± 0.01	-1.45 ± 0.00
Inc. Test LL	-8.87 ± 0.10	-3.38 ± 0.77	-9.48 ± 0.30	-5.10 ± 0.01	-5.24 ± 0.05	-10.77 ± 0.07	-4.73 ± 0.03	-6.63 ± 0.03
ECE	0.18 ± 0.00	0.10 ± 0.05	0.19 ± 0.00	0.14 ± 0.00	0.15 ± 0.00	0.19 ± 0.00	0.13 ± 0.00	0.15 ± 0.00

and we ensure that each model is trained using the same number of gradient steps to ensure a fair comparison. We evaluate each method using 20-fold cross-validation with 90/10 train/test splits.

We show train and test root mean square errors (RMSEs) and log likelihoods (LLs) in Fig. 3, and tabulate the log marginal likelihoods (LMLs) or ELBOs in Table 1. We make a few key observations. First, SVGP generally has similar metrics for both train and test datasets, indicating that the fit is well-calibrated. On the other hand, each of the deep methods suffers from some amount of overfitting for each dataset, and in many cases the overfitting for the DKL models is worse than for the pure NN models, reinforcing our observations on the toy problem. We also note that generally SVDKL overfits less than (V)DKL, and for BOSTON and ENERGY it performs better than the NNs on the test data. The exception to this trend is KIN40K, which appears to be low-noise and simple for a deep model to predict for. Finally, we note that, except for BOSTON, the DKL methods do not do significantly better than the NN methods in terms of log likelihoods, despite being able to model epistemic uncertainty, which the NN models cannot do.

It is well-known that minibatch training induces implicit regularization for neural networks that helps generalization [Keskar et al., 2016]. Our results suggest that stochastic minibatches may be important for the generalization of DKL models as well. Indeed, the difference between the full batch and stochastic minibatch performances of DKL seem to be greater than the corresponding differences for the standard neural networks, suggesting that the implicit regularization effect is stronger. Furthermore, Table 1 shows that the worse overfitting corresponds directly to better ELBOs/LMLs, indicating that the improved marginal likelihood is actually the cause of the worse generalization. Therefore, we observe again that the Bayesian benefits of the marginal likelihood do not apply in the overparameterized regime: indeed, we find that using the marginal likelihood can be worse than not being Bayesian at all.

6.2 DKL FOR IMAGE DATASETS

We now explore how these findings relate to high-dimensional, highly structure image datasets. We might expect that the benefits of DKL would be stronger for images than in the previous regression datasets, as the design of kernels for these high-dimensional spaces remains an open question despite numerous recent advances [Van der Wilk et al., 2017, Dutordoir et al., 2020].

We first consider a regression problem using image inputs: an age regression task using the UTKFace dataset [Zhang et al., 2017]. The dataset consists of 23,708 images of size $200 \times 200 \times 3$ containing aligned and cropped faces. These images are annotated with age, gender and race, of which we focus on the task of predicting the subject’s age.

We consider several models, all based on a ResNet-18 [He et al., 2016]: we take the standard ResNet-18 with 10-dimensional output, to which we add a ReLU nonlinearity and then either a linear output layer or an ARD SE GP, corresponding to the baseline neural network and SVDKL, respectively. We consider different feature widths Q in Appendix C. This construction ensures that both models have the same depth, so that any improvement observed for either cannot be attributed to the fact that the models have different depths. We consider the baseline neural network (NN) and SVDKL models. Additionally, as both Wilson et al. [2016a] and Bradshaw et al. [2017] use a pretraining and finetuning procedure for their models, we compare to this as well. We take the trained baseline NNs, and first learn the variational parameters and GP hyperparameters, keeping the network fixed. We refer to the result as the fixed net SVDKL (fSVDKL) model; we then train everything jointly for a number of epochs, resulting in the pretrained SVKDL (pSVDKL) model. Finally, so that any improvement for f/pSVDKL is not just from additional gradient steps, we also train the neural networks for the same number of epochs, resulting in the pretrained NN (pNN) model. We train all models with a batch size of 100, and we average all results over 3 independent runs. We refer the reader to App. B.3 for full experimental details.

Table 3: Results for the image datasets with data augmentation.

	Batch size: 100				Batch size: 200/500		
	NN	pNN	fSVDKL	pSVDKL	pNN	fSVDKL	pSVDKL
UTKFace - ELBO	-	-	0.16 ± 0.03	0.14 ± 0.03	-	0.12 ± 0.06	0.45 ± 0.03
Train RMSE	0.19 ± 0.01	0.18 ± 0.00	0.19 ± 0.00	0.17 ± 0.01	0.13 ± 0.00	0.20 ± 0.01	0.12 ± 0.01
Test RMSE	0.36 ± 0.00	0.36 ± 0.00	0.36 ± 0.00	0.35 ± 0.00	0.35 ± 0.00	0.31 ± 0.04	0.35 ± 0.01
Train LL	0.25 ± 0.03	0.31 ± 0.01	0.25 ± 0.03	0.30 ± 0.03	0.65 ± 0.02	0.20 ± 0.06	0.63 ± 0.04
Test LL	-1.03 ± 0.07	-1.22 ± 0.05	-0.92 ± 0.07	-0.76 ± 0.03	-2.72 ± 0.21	-0.63 ± 0.30	-1.55 ± 0.17
CIFAR-10 - ELBO	-	-	-0.07 ± 0.00	-0.03 ± 0.00	-	-0.06 ± 0.01	-0.01 ± 0.00
Train Acc.	0.98 ± 0.00	0.99 ± 0.00	0.99 ± 0.00	0.99 ± 0.00	1.00 ± 0.00	0.98 ± 0.00	1.00 ± 0.00
Test Acc.	0.86 ± 0.00	0.86 ± 0.00	0.86 ± 0.00	0.86 ± 0.00	0.87 ± 0.00	0.86 ± 0.00	0.86 ± 0.00
Train LL	-0.05 ± 0.00	-0.02 ± 0.00	-0.05 ± 0.00	-0.03 ± 0.00	-0.01 ± 0.00	-0.05 ± 0.01	-0.01 ± 0.00
Test LL	-0.70 ± 0.01	-0.90 ± 0.00	-0.68 ± 0.00	-0.64 ± 0.00	-1.38 ± 0.03	-0.67 ± 0.02	-0.84 ± 0.00
Inc. Test LL	-4.83 ± 0.12	-6.31 ± 0.00	-4.65 ± 0.00	-4.58 ± 0.00	-8.97 ± 0.07	-4.66 ± 0.13	-6.06 ± 0.01
ECE	0.09 ± 0.00	0.11 ± 0.00	0.09 ± 0.00	0.09 ± 0.00	0.12 ± 0.00	0.09 ± 0.00	0.11 ± 0.00

We report ELBOs, train and test RMSEs, and train and test log likelihoods for the normalized data in Table 2. We see that SVDKL obtains lower ELBOs than either fSVDKL or pSVDKL, which obtain largely similar ELBOs. We suspect that this is because of the difficulty in training large DKL models from scratch, as noted in Bradshaw et al. [2017]; this is also consistent with our earlier observation that training can be very unstable. We see that each method, except fSVDKL, achieves similar train RMSE, but the test RMSEs are significantly worse, with fSVDKL obtaining the best (although still within error bars of pSVDKL). Unsurprisingly, the NN models perform poorly in terms of LL, as they are unable to express epistemic uncertainty. However, we also observe that additional training of the NNs worsens both test RMSEs and LLs. pSVDKL obtains the best test LL of all methods, as well as better test RMSE than the neural networks, showing that SVDKL can yield improvements. We note, however, that there is still a substantial gap between train and test performance, indicating overfitting.

6.2.1 Increasing the Batch Size

From our UCI experiments, we hypothesized that implicit regularization from minibatch noise was key in obtaining good performance for SVDKL. We therefore consider increasing the batch size from 100 to 200 for the pretrained methods, keeping the pretrained neural networks the same; these results are also shown in Table 2. We make a few key observations. First, this leads to a significantly improved ELBO for pSVDKL, which helps the test RMSE. However, we see that instead of improving the test LL, it becomes significantly worse, whereas the train LL becomes better: clear evidence of overfitting. Moreover, fSVDKL, where the network is kept fixed, leading to a worse ELBO, now outperforms pSVDKL. Finally, we note that the behavior of pNN does not change significantly, in fact slightly improving with increased batch size: this suggests that the implicit regularization from minibatching is stronger for SVDKL than for standard NNs.

6.2.2 Image Classification

Our theory in Section 5 only applies directly to regression. As one of the main successes of current deep learning is in classification, it is therefore natural to wonder whether the trends we have observed also apply to classification tasks. We consider CIFAR-10 [Krizhevsky et al., 2009], a popular dataset of $32 \times 32 \times 3$ images belonging to one of 10 classes. We again consider a modified ResNet-18 model, in which we have ensured that the depths remain the same between NN and DKL models. We consider training the models with batch sizes of 100 and 500. We look at ELBOs, accuracies, and LLs, as well as the LL for incorrectly classified test points, which can indicate overconfidence in predicting wrongly, as well as expected calibration error (ECE; Guo et al. [2017]), a popular metric evaluating model calibration; results are shown again in Table 2. Here, we see that plain SVDKL struggles even more to fit well. For the batch size 100 experiments, pSVDKL generally performs the best, reflecting the experience of Wilson et al. [2016a] and Bradshaw et al. [2017]. However, we again observe that increasing the batch size hurts pSVDKL, and fSVDKL outperforms it.

6.3 DATA AUGMENTATION

It is common practice for image datasets to perform data augmentation, which effectively increases the size of the training dataset by using modified versions of the images. We briefly consider whether this affects our analysis by repeating the same experiments (without plain SVDKL, as it struggles to fit) with random cropping and horizontal flipping augmentations; see Table 3. Overall, we once again find that increasing the batch size still significantly hurts the performance of pSVDKL: whereas pSVDKL outperforms the fixed-network version for batch size 100, larger batch sizes reverse this, so that finetuning the network according to the ELBO hurts, rather than helps, performance. Therefore, in this case, using last-layer Bayesian inference is worse than not being Bayesian at all.

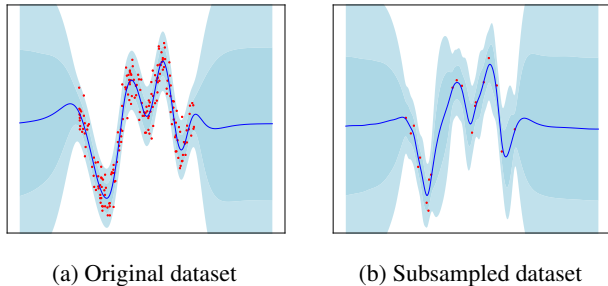


Figure 4: Predictive posteriors for fully Bayesian DKL using HMC for both the original toy dataset and the subsampled version from Titsias [2009].

Table 4: Results for the image datasets with SGLD.

	NN	SVDKL
UTKFace - Test RMSE	0.16 ± 0.00	0.16 ± 0.00
Test LL	0.39 ± 0.04	0.42 ± 0.03
CIFAR-10 - Test Acc.	0.79 ± 0.00	0.78 ± 0.00
Test LL	-1.89 ± 0.02	-1.11 ± 0.02
Inc. Test LL	-8.78 ± 0.11	-4.94 ± 0.10
ECE	0.18 ± 0.00	0.13 ± 0.00

7 ADDRESSING THE PATHOLOGY

We have seen that the empirical Bayesian approach to overparameterized Gaussian processes can lead to pathological behavior. In particular, we have shown that methods that rely on the marginal likelihood to optimize a large number of hyperparameters can overfit, and that learning is unstable. It is therefore natural to wonder whether we can address this by using a fully Bayesian approach, which has been shown to improve the predictive uncertainty of GP models [Lalchand and Rasmussen, 2020]. Indeed, Tran et al. [2019] showed that using Monte Carlo dropout to perform approximate Bayesian inference over the network parameters in DKL can improve calibration.

We test this hypothesis using sampling-based methods. We first consider the toy problem from earlier, using HMC [Neal et al., 2011] to sample the neural network weights along with the other GP hyperparameters, using the marginal likelihood as the potential. We plot the resulting predictive posterior in Fig. 4a, and see that this completely resolves the problems observed earlier: in fact, the uncertainty in the outer regions is even greater than that given by the standard SE fit in Fig. 1a, while still concentrating where there is data. We additionally consider the subsampled version of the dataset, as introduced in Titsias [2009], in Fig. 4b. We see that there is still no overfitting despite the small dataset size: for a comparison to the baseline SE kernel and DKL, see Fig. 5 in the Appendix.

Unfortunately, HMC in its standard form does not scale to the larger datasets considered in Sec. 6.2, due to the necessity of calculating gradients over the entire dataset and the calculation of the acceptance probability. Therefore, we consider stochastic gradient Langevin dynamics (SGLD; Welling and Teh [2011]), which allows us to use minibatches. While we do not necessarily expect that this will be as accurate to the true posterior as HMC (see e.g. Johndrow et al. [2020]), we hope that it will give insights into what the performance of a fully Bayesian approach would be. We select a batch size of 100, and give test results for the NN and SVDKL for both UTKFace and CIFAR-10 without data augmentation in Table 4. We see that for both datasets, the additional uncertainty significantly helps the NN models. The improvement is significant for SVDKL for the UTKFace dataset, and while not so significant for CIFAR-10, we still observe slight improvements in log likelihoods and ECE, although at the expense of slightly lower test accuracy. Moreover, the fully Bayesian SVDKL outperforms the Bayesian NN in nearly every metric, and significantly so for the uncertainty-related metrics. In fact, for CIFAR-10, the original version of SVDKL (i.e. pSVDKL) outperforms the Bayesian NN for the uncertainty metrics, even for the larger batch size experiments.

8 CONCLUSIONS

We have focused this work on exploring the performance of DKL in different regimes. We have shown that, while DKL models can achieve good performance, this is mostly because of implicit regularization due to stochastic mini-batching. Based off our experiments, this stochastic regularization appears to be stronger than that for plain neural networks. Moreover, we have shown that when this stochastic regularization is limited, the performance can be worse than that of standard neural networks, with more overfitting and unstable training. This is surprising, because DKL models are more Bayesian than deterministic neural networks, and so one might expect that they would be less prone to overfitting due to the training objective being the marginal likelihood. However, we have shown that for highly parameterized models, the marginal likelihood is actually a poor objective, as it tries to correlate all the datapoints rather than those which should be correlated: therefore, a higher marginal likelihood does not improve performance as expected. Finally, we showed that a fully Bayesian approach to the neural network hyperparameters can overcome this limitation and improve the performance over the less Bayesian approach, fully showing the advantages of DKL models.

Acknowledgements

We would like to thank John Bradshaw, David R. Burt, Andrew Y.K. Foong, Pola Elisabeth Schwöbel, and Andrew

Gordon Wilson for helpful discussions. SWO acknowledges the Gates Cambridge Trust for funding his doctoral studies.

References

- Martín Abadi, Ashish Agarwal, Paul Barham, Eugene Brevdo, Zhifeng Chen, Craig Citro, Greg S. Corrado, Andy Davis, Jeffrey Dean, Matthieu Devin, Sanjay Ghemawat, Ian Goodfellow, Andrew Harp, Geoffrey Irving, Michael Isard, Yangqing Jia, Rafal Jozefowicz, Lukasz Kaiser, Manjunath Kudlur, Josh Levenberg, Dandelion Mané, Rajat Monga, Sherry Moore, Derek Murray, Chris Olah, Mike Schuster, Jonathon Shlens, Benoit Steiner, Ilya Sutskever, Kunal Talwar, Paul Tucker, Vincent Vanhoucke, Vijay Vasudevan, Fernanda Viégas, Oriol Vinyals, Pete Warden, Martin Wattenberg, Martin Wicke, Yuan Yu, and Xiaoqiang Zheng. TensorFlow: Large-scale machine learning on heterogeneous systems, 2015. URL <https://www.tensorflow.org/>. Software available from tensorflow.org.
- John Bradshaw, Alexander G de G Matthews, and Zoubin Ghahramani. Adversarial examples, uncertainty, and transfer testing robustness in Gaussian process hybrid deep networks. *arXiv preprint arXiv:1707.02476*, 2017.
- David R Burt, Carl Edward Rasmussen, and Mark van der Wilk. Convergence of sparse variational inference in Gaussian processes regression. *Journal of Machine Learning Research*, 21:1–63, 2020.
- Roberto Calandra, Jan Peters, Carl Edward Rasmussen, and Marc Peter Deisenroth. Manifold Gaussian processes for regression. In *2016 International Joint Conference on Neural Networks (IJCNN)*, pages 3338–3345. IEEE, 2016.
- Luis Pedro Coelho. Jug: Software for parallel reproducible computation in python. *Journal of Open Research Software*, 5(1), 2017.
- Dheeru Dua and Casey Graff. UCI machine learning repository, 2017. URL <http://archive.ics.uci.edu/ml>.
- Michael Dusenberry, Ghassen Jerfel, Yeming Wen, Yian Ma, Jasper Snoek, Katherine Heller, Balaji Lakshminarayanan, and Dustin Tran. Efficient and scalable Bayesian neural nets with rank-1 factors. In *International conference on machine learning*, pages 2782–2792. PMLR, 2020.
- Vincent Dutordoir, Mark Wilk, Artem Artemev, and James Hensman. Bayesian image classification with deep convolutional Gaussian processes. In *International Conference on Artificial Intelligence and Statistics*, pages 1529–1539. PMLR, 2020.
- Yarin Gal and Zoubin Ghahramani. Dropout as a Bayesian approximation: Representing model uncertainty in deep learning. In *international conference on machine learning*, pages 1050–1059. PMLR, 2016.
- Chuan Guo, Geoff Pleiss, Yu Sun, and Kilian Q Weinberger. On calibration of modern neural networks. In *International Conference on Machine Learning*, pages 1321–1330. PMLR, 2017.
- Kaiming He, Xiangyu Zhang, Shaoqing Ren, and Jian Sun. Deep residual learning for image recognition. In *Proceedings of the IEEE conference on computer vision and pattern recognition*, pages 770–778, 2016.
- Jonathan Heek and Nal Kalchbrenner. Bayesian inference for large scale image classification. *arXiv preprint arXiv:1908.03491*, 2019.
- James Hensman, Alexander Matthews, and Zoubin Ghahramani. Scalable variational Gaussian process classification. In *Artificial Intelligence and Statistics*, pages 351–360. PMLR, 2015a.
- James Hensman, Alexander G de G Matthews, Maurizio Filippone, and Zoubin Ghahramani. Mcmc for variationally sparse Gaussian processes. *arXiv preprint arXiv:1506.04000*, 2015b.
- Sergey Ioffe and Christian Szegedy. Batch normalization: Accelerating deep network training by reducing internal covariate shift. In *International conference on machine learning*, pages 448–456. PMLR, 2015.
- James E Johndrow, Natesh S Pillai, and Aaron Smith. No free lunch for approximate mcmc. *arXiv preprint arXiv:2010.12514*, 2020.
- Nitish Shirish Keskar, Dheevatsa Mudigere, Jorge Nocedal, Mikhail Smelyanskiy, and Ping Tak Peter Tang. On large-batch training for deep learning: Generalization gap and sharp minima. *arXiv preprint arXiv:1609.04836*, 2016.
- Diederik P Kingma and Jimmy Ba. Adam: A method for stochastic optimization. *arXiv preprint arXiv:1412.6980*, 2014.
- Diederik P Kingma and Max Welling. Auto-encoding variational bayes. *arXiv preprint arXiv:1312.6114*, 2013.
- Alex Krizhevsky, Geoffrey Hinton, et al. Learning multiple layers of features from tiny images. 2009.
- Vidhi Lalchand and Carl Edward Rasmussen. Approximate inference for fully Bayesian Gaussian process regression. In *Symposium on Advances in Approximate Bayesian Inference*, pages 1–12. PMLR, 2020.
- Yann LeCun, Yoshua Bengio, and Geoffrey Hinton. Deep learning. *nature*, 521(7553):436–444, 2015.

- Jeremiah Zhe Liu, Zi Lin, Shreyas Padhy, Dustin Tran, Tania Bedrax-Weiss, and Balaji Lakshminarayanan. Simple and principled uncertainty estimation with deterministic deep learning via distance awareness. *arXiv preprint arXiv:2006.10108*, 2020.
- Alexander G. de G. Matthews, Mark van der Wilk, Tom Nickson, Keisuke Fujii, Alexis Boukouvalas, Pablo León-Villagrà, Zoubin Ghahramani, and James Hensman. GPflow: A Gaussian process library using TensorFlow. *Journal of Machine Learning Research*, 18(40): 1–6, apr 2017. URL <http://jmlr.org/papers/v18/16-537.html>.
- Radford M Neal et al. Mcmc using hamiltonian dynamics. *Handbook of markov chain monte carlo*, 2(11):2, 2011.
- Sebastian W Ober and Laurence Aitchison. Global inducing point variational posteriors for Bayesian neural networks and deep Gaussian processes. *arXiv preprint arXiv:2005.08140*, 2020.
- Sebastian W Ober and Carl Edward Rasmussen. Benchmarking the neural linear model for regression. *arXiv preprint arXiv:1912.08416*, 2019.
- Kazuki Osawa, Siddharth Swaroop, Anirudh Jain, Runa Eschenhagen, Richard E Turner, Rio Yokota, and Mohammad Emtiyaz Khan. Practical deep learning with Bayesian principles. *arXiv preprint arXiv:1906.02506*, 2019.
- Carl Edward Rasmussen and Christopher KI Williams. *Gaussian Processes for Machine Learning*. ISBN-13 978-0-262-18253-9, 2006.
- Danilo Jimenez Rezende, Shakir Mohamed, and Daan Wierstra. Stochastic backpropagation and approximate inference in deep generative models. In *International conference on machine learning*, pages 1278–1286. PMLR, 2014.
- Carlos Riquelme, George Tucker, and Jasper Snoek. Deep Bayesian bandits showdown: An empirical comparison of Bayesian deep networks for thompson sampling. *arXiv preprint arXiv:1802.09127*, 2018.
- Ruslan Salakhutdinov and Geoffrey E Hinton. Using deep belief nets to learn covariance kernels for Gaussian processes. In *NIPS*, volume 7, pages 1249–1256. Citeseer, 2007.
- Hugh Salimbeni and Marc Deisenroth. Doubly stochastic variational inference for deep Gaussian processes. *arXiv preprint arXiv:1705.08933*, 2017.
- Edward Snelson and Zoubin Ghahramani. Sparse Gaussian processes using pseudo-inputs. In *Advances in neural information processing systems*, pages 1257–1264, 2006.
- Michalis Titsias. Variational learning of inducing variables in sparse Gaussian processes. In *Artificial Intelligence and Statistics*, pages 567–574, 2009.
- Gia-Lac Tran, Edwin V Bonilla, John Cunningham, Pietro Michiardi, and Maurizio Filippone. Calibrating deep convolutional Gaussian processes. In *The 22nd International Conference on Artificial Intelligence and Statistics*, pages 1554–1563. PMLR, 2019.
- Joost van Amersfoort, Lewis Smith, Yee Whye Teh, and Yarin Gal. Simple and scalable epistemic uncertainty estimation using a single deep deterministic neural network. *arXiv preprint arXiv:2003.02037*, 2020.
- Mark Van der Wilk, Carl Edward Rasmussen, and James Hensman. Convolutional Gaussian processes. *arXiv preprint arXiv:1709.01894*, 2017.
- Max Welling and Yee W Teh. Bayesian learning via stochastic gradient langevin dynamics. In *Proceedings of the 28th international conference on machine learning (ICML-11)*, pages 681–688. Citeseer, 2011.
- Andrew Wilson and Hannes Nickisch. Kernel interpolation for scalable structured Gaussian processes (kiss-gp). In *International Conference on Machine Learning*, pages 1775–1784. PMLR, 2015.
- Andrew G Wilson, Zhiting Hu, Russ R Salakhutdinov, and Eric P Xing. Stochastic variational deep kernel learning. In *Advances in Neural Information Processing Systems*, pages 2586–2594, 2016a.
- Andrew Gordon Wilson, Christoph Dann, and Hannes Nickisch. Thoughts on massively scalable Gaussian processes. *arXiv preprint arXiv:1511.01870*, 2015.
- Andrew Gordon Wilson, Zhiting Hu, Ruslan Salakhutdinov, and Eric P Xing. Deep kernel learning. In *Artificial intelligence and statistics*, pages 370–378, 2016b.
- Ruqi Zhang, Chunyuan Li, Jianyi Zhang, Changyou Chen, and Andrew Gordon Wilson. Cyclical stochastic gradient mcmc for Bayesian deep learning. *arXiv preprint arXiv:1902.03932*, 2019.
- Zhifei Zhang, Yang Song, and Hairong Qi. Age progression/regression by conditional adversarial autoencoder. In *IEEE Conference on Computer Vision and Pattern Recognition (CVPR)*. IEEE, 2017.

A PROOF OF PROPOSITION 1

We restate the proposition:

Proposition 1. *Consider the Gaussian process regression model as described in Eq. 1. Then, for any valid kernel function that can be written in the form $k(x, x') = \sigma_f^2 \hat{k}(x, x')$, where σ_f^2 is a learnable hyperparameter along with learnable noise σ_n^2 (and any other kernel hyperparameters), we have that the “data fit” term will equal $-N/2$ at the optimum of the marginal likelihood.*

Proof. We reparameterize $\sigma_n^2 = \hat{\sigma}_n^2 \sigma_f^2$. Then, writing $K + \sigma_n^2 I_N = \sigma_f^2 (\hat{K} + \hat{\sigma}_n^2 I_N)$, the result follows by differentiating the log marginal likelihood with respect to σ_f^2 :

$$\begin{aligned} \frac{d}{d\sigma_f^2} \log p(\mathbf{y}) &= \frac{d}{d\sigma_f^2} \left(-\frac{N}{2} \log \sigma_f^2 - \frac{1}{2} \log |\hat{K} + \hat{\sigma}_n^2 I_N| - \frac{1}{2\sigma_f^2} \mathbf{y}^T (\hat{K} + \hat{\sigma}_n^2 I_N)^{-1} \mathbf{y} \right) \\ &= -\frac{N}{2\sigma_f^2} + \frac{1}{2\sigma_f^4} \mathbf{y}^T (\hat{K} + \hat{\sigma}_n^2 I_N)^{-1} \mathbf{y}. \end{aligned}$$

Setting the derivative equal to zero gives:

$$\sigma_f^2 = \frac{1}{N} \mathbf{y}^T (\hat{K} + \hat{\sigma}_n^2 I_N)^{-1} \mathbf{y}.$$

Substituting this into the data fit term gives the desired result. \square

B EXPERIMENTAL DETAILS

All experiments on real datasets (UCI, CIFAR-10, UTKFace) were written in TensorFlow 2 [Abadi et al., 2015], using GPflow [Matthews et al., 2017] to implement the DKL models. We use jug [Coelho, 2017] to easily run the experiments. The experiments were run on single GPUs using both NVIDIA Tesla P100-PCIE-16GB GPUs and NVIDIA GeForce RTX 2080 Ti GPUs.

B.1 DATASETS

We describe the datasets used as well as the splits and preprocessing.

Toy dataset The toy dataset is that as introduced in Snelson and Ghahramani [2006], which was generated from a function realization sampled from a SE GP. The dataset comprises 200 input-output pairs and can be found at <http://www.gatsby.ucl.ac.uk/~snelson/>. We normalize both inputs and outputs for training and plot the unnormalized values and predictions.

UCI We use a slightly modified version of Bayesian Benchmarks (https://github.com/hughsalimbeni/bayesian_benchmarks) to obtain the UCI datasets we use. The modification is to rectify minor data leakage in the normalization code: they normalize using the statistics from the entire dataset before dividing into train/test splits, instead of normalizing using only the train split statistics. We perform cross-validation using 20 90%/10% train/test splits, and report means and standard errors for each metric. Note that we report metrics on the normalized datasets to lead to more interpretable results: namely, an RMSE of 1 corresponds to predicting 0 for each test point.

CIFAR-10 We use the standard CIFAR-10 dataset [Krizhevsky et al., 2009], with the standard train-validation split of 50,000 and 10,000 images, respectively, using the validation split as the test set, as is common practice. We preprocess the images by simply dividing the pixel values by 255, so that each value lies between 0 and 1.

UTKFace The UTKFace dataset [Zhang et al., 2017] is a large face dataset consisting of 23,708 images of faces, annotated with age, gender, and ethnicity. The faces have an age range from 0 to 116. We use the aligned and cropped version to limit the amount of preprocessing necessary, available at <https://susanqq.github.io/UTKFace/>. These cropped images have sizes $200 \times 200 \times 3$. We choose 20,000 images to be in the train dataset, with the remaining being used for testing. We again perform preprocessing by dividing the pixel values by 255, and we additionally normalize the age values. The metrics we report all use the normalized values, as with the UCI datasets.

B.2 MODELS

We describe the models used for the experiments. To ensure that the comparisons between neural networks and DKL models are as fair as possible, we ensure that each model used in direct comparison has the same number of layers: for the DKL models, we remove the last fully-connected layer of the neural network and replace it with the ARD SE GP. All neural networks use ReLU activations. For all SVDKL models, the inducing points live in the neural network feature space at the input to the GP.

Toy dataset We use an architecture of $[100, 50, 2]$ for the hidden-layer widths for the neural network. For DKL, we use the pre-activation features of the final hidden layer for the input to the GP.

UCI For BOSTON, ENERGY, we use an architecture of $[50, 50]$, and an architecture $[1000, 500, 50]$ for KIN40K, POWER, and PROTEIN. For the DKL models, we use the post-activation features from the final hidden layer as inputs to the GPs, which use ARD SE kernels. For SVDKL, we initialize the inducing points using the k-means algorithm on a subset of the training set. We use 100 inducing points for the smaller datasets (BOSTON, ENERGY) and 1000 on the larger ones. The method for initializing the inducing points, and the number of inducing points, is the same for the SVGP baseline model, which uses a standard ARD SE kernel.

CIFAR-10 We use a modified ResNet18 [He et al., 2016] architecture as the baseline neural network architecture; the main modification is that we have added another fully-connected layer at the output to ensure that the neural network and DKL models are comparable in depth. Therefore, instead of the standard single fully-connected layer after a global average pooling layer, we have two fully-connected layers. While we could take the output of the global average pooling layer, this is typically very high-dimensional and thus potentially unsuitable as an input to a GP. For most experiments, we fix the width of the last hidden layer (the final feature width) to 10, although we do consider changing that in App. C. We additionally add batchnorm layers [Ioffe and Szegedy, 2015] before the ReLU activations in the residual blocks. For SVDKL, we use 1000 inducing points initialized with k-means on a subset of the training set. As with UCI, the features at the input to the GP are post-activation features. For all classification models, we use softmax activation to obtain probabilities for the cross-entropy loss, and for the SVDKL models we use 10 samples from the latent function posterior to compute the log likelihood term of the ELBO.

UTKFace As with CIFAR-10, we again use a modified ResNet18 [He et al., 2016] architecture with an additional fully-connected layer at the output. For SVDKL, we again use 1000 inducing points.

B.3 IMPLEMENTATION DETAILS

All models are optimized using ADAM [Kingma and Ba, 2014]. Throughout, we try to ensure that we train each model for comparable numbers of gradient steps and learning rates.

Toy dataset We train both the NN and DKL models in for 10,000 gradient steps using learning rates of 0.001. No weight decay was used. For the HMC experiments, we use a step size of 0.005, 20 leapfrog steps, and a prior variance of 1 on the network weights. We burn in for 10,000 samples, then use 1,000 iterations to sample, thinned by a factor of 10.

UCI For each model, we train with an initial learning rate of 0.001. For BOSTON and ENERGY, we use a batch size of 32 and train the minibatched algorithms for a total of 400 epochs, and use a learning rate scheduler that decreases the learning rate by a factor of 10 after 200 and 300 epochs. For KIN40K, POWER, and PROTEIN we use a batch size of 100, training for 160 epochs with the same learning rate schedule that triggers at 80 and 120 epochs. For the full-batch methods, we ensure that they are trained for the lesser of the same number of gradient steps or 8000 gradient steps (due to limited computational budget), with the learning rate schedule set to trigger at the corresponding number of gradient steps as the batched methods. This ensures a fair comparison when claiming that the full-batch methods overfit in comparison to the stochastic versions. For the deep models, we use a weight decay of $1e-4$ on the neural network weights. We do not use any pretraining for the DKL models, as we did not find it necessary for these datasets. We initialize the log noise variance to -4 for the DKL models. We train the neural network models using mean squared error loss, and use the maximum likelihood noise estimate after training to compute train and test log likelihoods.

CIFAR-10 We describe the details for batch size 100; for batch size 500, we ensure that we use the same number of gradient steps. We do not use weight decay as we found that it hurt test accuracy. For NN and SVDKL, we train for 160 epochs total: we decrease the learning rate from the initial $1e-3$ by a factor of 10 at 80 and then 120 epochs. For pNN, we train for an additional 160 epochs in the same way (restarting the learning rate at $1e-3$). For pSVDKL, we start by training with the neural network parameters fixed for 80 epochs, with learning rate decreases at 40 and 60 epochs. We then reset the learning rate to $1e-3$, and train for an additional 80 epochs with learning rate decreases at 40 and 60 epochs. For the experiments with data augmentation, we use random horizontal flipping and randomly crop $32 \times 32 \times 3$ images from the original images padded up to $40 \times 40 \times 3$.

We use the same losses as the potentials for SGLD. We use the trained NNs to initialize the weights to reasonable values, and set the batch size to 100. We initialize the learning rate to $1e-3$ (which we then scale down by the dataset size to account for the scale of the potential), and decay the learning rate at each epoch by a factor of $1/(1 + 0.4 \times \text{epoch})$ to satisfy Robbins-Monro. For the NN, we burn in for 100 epochs, and then sample every other epoch for 100 epochs, leading to 50 samples. For SVDKL, we follow the approach in Hensman et al. [2015b], and learn the variational parameters (i.e. 1000 inducing points) and GP hyperparameters with the fixed, pretrained NN weights, using the same hyperparameters as for pSVDKL. We then follow the SGLD approach we took for the NN, with 100 epochs of burn in and 100 epochs of sampling, starting with a learning rate of $1e-3$.

UTKFace We follow the same approach as for CIFAR-10. We list the minor differences. We use a small weight decay of $1e-4$. For the SVDKL models, we initialize the log noise variance to -4. We use mean squared error loss for the NNs; however, for SGLD we use a Gaussian likelihood with log noise variance initialized to -4. For the SGLD experiments, we initialize the learning rate to $1e-5$. For data augmentation, we again use random horizontal flipping as well as randomly cropping $200 \times 200 \times 3$ images from the original images padded up to $240 \times 240 \times 3$.

C ADDITIONAL EXPERIMENTAL RESULTS

Here we briefly present some additional experimental results.

C.1 TOY

We show additional plots of fits and training curves for the toy problem from Snelson and Ghahramani [2006] in Fig. 5. Below the fits, we again show the kernel correlation at two different points x' , marked by the vertical dashed lines. In Figure 5a, we show the fit using the standard squared exponential kernel, followed by two fits using DKL in Figures 5b and 5c. In Fig. 5d we show training curves for 5 different initializations; note that unlike in the main text we use a learning rate of $1e-4$ here and so require more training iterations to converge. Finally, we consider plots of fits on the subsampled version of the dataset as in Titsias [2009]; we show fits using the SE kernel and DKL in Figures 5e and 5f, respectively. For each fit, we also show the log marginal likelihood in the caption.

We make a few observations. First, note that different initializations can lead to very different fits and LMLs. Moreover, as predicted by our theory, the highest log marginal likelihoods are obtained when the prior attempts to correlate all the points in the input domain: Fig. 5b obtains a higher LML than Fig. 5c. However, instability in training often leads to worse LMLs than could be obtained (Fig. 5d). Finally, we note that the overfitting is substantially worse on the subsampled version of the dataset: we also see that the prior is more correlated than previously (Fig. 5f).

C.2 CHANGING THE FEATURE DIMENSION

We perform experiments changing the feature dimension Q for the UTKFace and CIFAR-10 datasets. We present the results in Tables 5 and 6, where each model name is followed by the feature space dimension. For UTKFace, it is clear that 2 neurons is not sufficient to fit the data. Beyond 2, we see only minor changes in performance. For CIFAR-10, we find that we need at least 10 neurons to fit well, but beyond 10 there are again only minor differences. We choose 10 neurons for both experiments out of convenience.

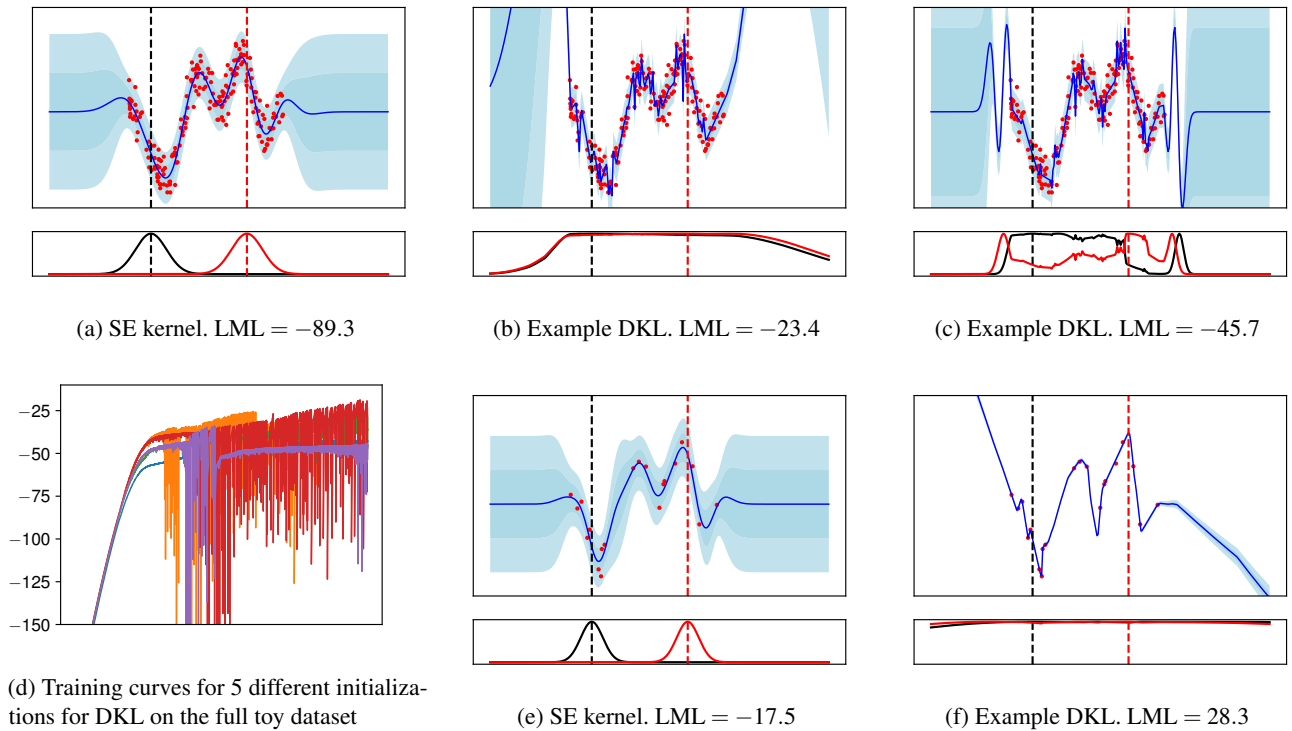


Figure 5: Plots of fits and training curves using standard SE kernel and DKL. Below each fit we plot two correlation functions $\rho_{x'}(x) = k(x, x') / \sigma_f^2$ induced by each kernel, where the location of x' is given by the dashed vertical lines. (a)-(d) show fits and training curves for the full toy dataset introduced in Snelson and Ghahramani [2006], whereas (e)-(f) show fits on the subsampled version from Titsias [2009].

Table 5: Results for UTKFace.

	ELBO	Train RMSE	Test RMSE	Train LL	Test LL
NN-2	-	0.37 ± 0.26	0.61 ± 0.16	0.58 ± 0.82	-23.14 ± 10.94
SVDKL-2	-0.22 ± 1.00	0.39 ± 0.25	0.61 ± 0.16	0.14 ± 0.68	-3.60 ± 1.90
pNN-2	-	0.36 ± 0.26	0.61 ± 0.16	0.74 ± 0.88	-35.66 ± 14.00
fSVDKL-2	-0.32 ± 4.00	0.45 ± 0.22	0.45 ± 0.23	-0.26 ± 0.50	-0.23 ± 0.52
pSVDKL-2	0.36 ± 3.00	0.36 ± 0.26	0.53 ± 0.20	0.47 ± 0.77	-3.24 ± 0.76
NN-5	-	0.04 ± 0.00	0.41 ± 0.01	1.72 ± 0.05	-42.86 ± 2.79
SVDKL-5	-0.17 ± 0.59	0.11 ± 0.01	0.47 ± 0.01	0.40 ± 0.11	-1.41 ± 0.16
pNN-5	-	0.04 ± 0.00	0.41 ± 0.00	1.79 ± 0.01	-48.92 ± 0.62
fSVDKL-5	0.31 ± 0.48	0.17 ± 0.00	0.17 ± 0.00	0.38 ± 0.02	0.37 ± 0.03
pSVDKL-5	0.99 ± 0.73	0.04 ± 0.00	0.32 ± 0.01	1.18 ± 0.06	-2.61 ± 0.26
NN-10	-	0.04 ± 0.00	0.40 ± 0.00	1.81 ± 0.01	-48.73 ± 1.64
SVDKL-10	0.92 ± 0.15	0.04 ± 0.00	0.40 ± 0.01	1.30 ± 0.01	-6.88 ± 0.38
pNN-10	-	0.04 ± 0.00	0.41 ± 0.00	1.83 ± 0.01	-53.72 ± 1.71
fSVDKL-10	1.05 ± 0.02	0.08 ± 0.03	0.31 ± 0.07	1.16 ± 0.31	-7.55 ± 3.42
pSVDKL-10	1.03 ± 0.07	0.04 ± 0.00	0.38 ± 0.02	1.20 ± 0.08	-4.74 ± 1.35
NN-20	-	0.04 ± 0.00	0.40 ± 0.00	1.78 ± 0.01	-46.77 ± 1.72
SVDKL-20	0.22 ± 0.01	0.08 ± 0.02	0.43 ± 0.01	0.78 ± 0.22	-3.42 ± 1.52
pNN-20	-	0.04 ± 0.00	0.41 ± 0.00	1.80 ± 0.01	-50.51 ± 0.47
fSVDKL-20	0.71 ± 0.30	0.12 ± 0.03	0.24 ± 0.06	0.83 ± 0.34	-5.06 ± 4.46
pSVDKL-20	1.15 ± 0.10	0.04 ± 0.00	0.34 ± 0.03	1.33 ± 0.04	-4.16 ± 0.42
NN-50	-	0.04 ± 0.00	0.40 ± 0.00	1.79 ± 0.01	-47.72 ± 0.68
SVDKL-50	0.92 ± 0.27	0.04 ± 0.00	0.40 ± 0.00	1.33 ± 0.03	-7.35 ± 0.45
pNN-50	-	0.04 ± 0.00	0.41 ± 0.01	1.81 ± 0.00	-51.14 ± 1.33
fSVDKL-50	1.14 ± 0.31	0.08 ± 0.03	0.32 ± 0.06	1.29 ± 0.35	-11.60 ± 4.91
pSVDKL-50	1.21 ± 0.03	0.04 ± 0.00	0.37 ± 0.02	1.37 ± 0.02	-5.71 ± 0.55

Table 6: Results for CIFAR-10.

	ELBO	Train Acc.	Test Acc.	Train LL	Test LL	Inc. Test LL	ECE
NN-2	-	0.69 ± 0.24	0.51 ± 0.17	-0.81 ± 0.61	-6.42 ± 2.23	-6.40 ± 1.78	0.14 ± 0.06
SVDKL-2	-1.38 ± 0.38	0.52 ± 0.17	0.46 ± 0.15	-1.34 ± 0.39	-1.57 ± 0.30	-2.61 ± 0.13	0.04 ± 0.02
pNN-2	-	0.70 ± 0.24	0.53 ± 0.17	-0.77 ± 0.63	-5.25 ± 1.36	-7.28 ± 2.03	0.15 ± 0.06
fSVDKL-2	-0.85 ± 0.59	0.69 ± 0.24	0.51 ± 0.17	-0.81 ± 0.61	-1.83 ± 0.20	-4.35 ± 0.84	0.14 ± 0.06
pSVDKL-2	-0.78 ± 0.62	0.70 ± 0.24	0.53 ± 0.17	-0.78 ± 0.62	-1.76 ± 0.23	-4.51 ± 0.90	0.13 ± 0.05
NN-5	-	0.70 ± 0.25	0.55 ± 0.18	-0.77 ± 0.63	-3.03 ± 0.58	-7.00 ± 1.92	0.13 ± 0.05
SVDKL-5	-1.66 ± 0.26	0.40 ± 0.12	0.39 ± 0.12	-1.63 ± 0.28	-1.68 ± 0.25	-2.30 ± 0.00	0.02 ± 0.01
pNN-5	-	0.70 ± 0.25	0.55 ± 0.18	-0.77 ± 0.63	-3.22 ± 0.68	-7.34 ± 2.06	0.13 ± 0.05
fSVDKL-5	-0.79 ± 0.62	0.70 ± 0.24	0.55 ± 0.18	-0.77 ± 0.63	-1.61 ± 0.29	-4.25 ± 0.80	0.09 ± 0.04
pSVDKL-5	-0.77 ± 0.62	0.70 ± 0.24	0.55 ± 0.19	-0.77 ± 0.63	-1.64 ± 0.27	-4.66 ± 0.96	0.11 ± 0.04
NN-10	-	1.00 ± 0.00	0.79 ± 0.00	-0.00 ± 0.00	-2.05 ± 0.03	-8.87 ± 0.10	0.18 ± 0.00
SVDKL-10	-0.76 ± 0.28	0.76 ± 0.09	0.63 ± 0.03	-0.71 ± 0.28	-1.37 ± 0.10	-3.38 ± 0.77	0.10 ± 0.05
pNN-10	-	1.00 ± 0.00	0.79 ± 0.00	-0.00 ± 0.00	-2.30 ± 0.11	-9.48 ± 0.30	0.19 ± 0.00
fSVDKL-10	-0.02 ± 0.00	1.00 ± 0.00	0.78 ± 0.00	-0.01 ± 0.00	-1.14 ± 0.00	-5.10 ± 0.01	0.14 ± 0.00
pSVDKL-10	-0.00 ± 0.00	1.00 ± 0.00	0.79 ± 0.00	-0.00 ± 0.00	-1.13 ± 0.01	-5.24 ± 0.05	0.15 ± 0.00
NN-20	-	1.00 ± 0.00	0.79 ± 0.00	-0.00 ± 0.00	-2.06 ± 0.02	-8.91 ± 0.14	0.18 ± 0.00
SVDKL-20	-0.30 ± 0.20	0.91 ± 0.06	0.70 ± 0.02	-0.26 ± 0.19	-1.46 ± 0.16	-4.72 ± 0.88	0.16 ± 0.04
pNN-20	-	1.00 ± 0.00	0.79 ± 0.00	-0.00 ± 0.00	-2.24 ± 0.01	-9.37 ± 0.08	0.19 ± 0.00
fSVDKL-20	-0.02 ± 0.00	1.00 ± 0.00	0.79 ± 0.00	-0.01 ± 0.00	-1.14 ± 0.02	-5.16 ± 0.10	0.13 ± 0.00
pSVDKL-20	-0.00 ± 0.00	1.00 ± 0.00	0.79 ± 0.00	-0.00 ± 0.00	-1.09 ± 0.01	-5.12 ± 0.05	0.15 ± 0.00
NN-50	-	1.00 ± 0.00	0.79 ± 0.00	-0.00 ± 0.00	-2.18 ± 0.01	-9.23 ± 0.04	0.19 ± 0.00
SVDKL-50	-2.30 ± 0.00	0.10 ± 0.00	0.10 ± 0.00	-2.30 ± 0.00	-2.30 ± 0.00	-2.30 ± 0.00	0.00 ± 0.00
pNN-50	-	1.00 ± 0.00	0.79 ± 0.00	-0.00 ± 0.00	-2.38 ± 0.06	-9.73 ± 0.15	0.19 ± 0.00
fSVDKL-50	-0.02 ± 0.00	1.00 ± 0.00	0.79 ± 0.00	-0.00 ± 0.00	-1.22 ± 0.01	-5.48 ± 0.05	0.14 ± 0.00
pSVDKL-50	-0.00 ± 0.00	1.00 ± 0.00	0.79 ± 0.00	-0.00 ± 0.00	-1.11 ± 0.01	-5.13 ± 0.04	0.15 ± 0.00

D TABULATED UCI RESULTS

Here we tabulate the results for the UCI datasets.

Table 7: Results for BOSTON. We report means plus or minus one standard error averaged over the splits.

	loss	train RMSE	test RMSE	train LL	test LL
SVGP	1.66 ± 0.06	0.39 ± 0.01	0.37 ± 0.02	-0.34 ± 0.01	-0.33 ± 0.05
fNN	0.01 ± 0.00	0.02 ± 0.00	0.39 ± 0.03	2.28 ± 0.03	-132.41 ± 22.39
sNN	0.01 ± 0.00	0.10 ± 0.00	0.34 ± 0.02	0.93 ± 0.02	-5.61 ± 1.03
DKL	-2.47 ± 0.00	0.00 ± 0.00	0.41 ± 0.02	2.72 ± 0.00	-67.55 ± 3.97
SVDKL	-0.47 ± 0.01	0.13 ± 0.00	0.35 ± 0.02	0.57 ± 0.01	-1.12 ± 0.24

Table 8: Results for ENERGY.

	loss	train RMSE	test RMSE	train LL	test LL
SVGP	0.07 ± 0.01	0.19 ± 0.00	0.20 ± 0.00	0.19 ± 0.01	0.15 ± 0.02
fNN	0.00 ± 0.00	0.02 ± 0.00	0.04 ± 0.00	2.55 ± 0.02	-0.04 ± 0.38
sNN	0.00 ± 0.00	0.02 ± 0.00	0.05 ± 0.00	2.31 ± 0.02	0.62 ± 0.19
DKL	-3.01 ± 0.02	0.01 ± 0.00	0.05 ± 0.00	3.15 ± 0.02	-2.63 ± 0.49
SVDKL	-1.21 ± 0.00	0.03 ± 0.00	0.04 ± 0.00	1.26 ± 0.00	1.22 ± 0.01

Table 9: Results for KIN40K.

	loss	train RMSE	test RMSE	train LL	test LL
SVGP	-0.14 ± 0.00	0.16 ± 0.00	0.17 ± 0.00	0.36 ± 0.00	0.33 ± 0.00
fNN	0.01 ± 0.00	0.03 ± 0.00	0.05 ± 0.00	2.18 ± 0.00	1.17 ± 0.02
sNN	0.01 ± 0.00	0.03 ± 0.00	0.05 ± 0.00	2.03 ± 0.00	1.51 ± 0.01
VDKL	-1.41 ± 0.00	0.02 ± 0.00	0.05 ± 0.00	1.44 ± 0.00	1.33 ± 0.00
SVDKL	-2.62 ± 0.00	0.01 ± 0.00	0.03 ± 0.00	2.68 ± 0.00	1.73 ± 0.02

Table 10: Results for POWER.

	loss	train RMSE	test RMSE	train LL	test LL
SVGP	-0.01 ± 0.00	0.23 ± 0.00	0.23 ± 0.00	0.06 ± 0.00	0.07 ± 0.01
fNN	0.04 ± 0.00	0.17 ± 0.00	0.21 ± 0.00	0.37 ± 0.00	0.11 ± 0.02
sNN	0.05 ± 0.00	0.21 ± 0.00	0.22 ± 0.00	0.14 ± 0.00	0.11 ± 0.01
VDKL	-0.57 ± 0.00	0.13 ± 0.00	0.21 ± 0.00	0.62 ± 0.00	-0.02 ± 0.02
SVDKL	-0.25 ± 0.00	0.18 ± 0.00	0.21 ± 0.00	0.28 ± 0.00	0.16 ± 0.01

Table 11: Results for PROTEIN.

	loss	train RMSE	test RMSE	train LL	test LL
SVGP	1.06 ± 0.00	0.64 ± 0.00	0.66 ± 0.00	-0.98 ± 0.00	-1.00 ± 0.00
fNN	0.19 ± 0.00	0.39 ± 0.00	0.58 ± 0.00	-0.46 ± 0.00	-1.09 ± 0.01
sNN	0.17 ± 0.00	0.35 ± 0.00	0.55 ± 0.00	-0.36 ± 0.00	-1.14 ± 0.01
VDKL	0.32 ± 0.01	0.30 ± 0.00	0.59 ± 0.00	-0.23 ± 0.01	-1.86 ± 0.01
SVDKL	0.35 ± 0.00	0.31 ± 0.00	0.57 ± 0.00	-0.26 ± 0.00	-1.29 ± 0.01